Review of Scientific Instruments

Spatial and temporal pre-alignment of an X-ray split-and-delay unit by laser light interferometry

Cite as: Rev. Sci. Instrum. **90**, 045106 (2019); https://doi.org/10.1063/1.5089496
Submitted: 19 January 2019 . Accepted: 15 March 2019 . Published Online: 04 April 2019

W. Roseker, S. Lee, M. Walther, R. Rysov, M. Sprung, and G. Grübel

Review of Scientific Instruments ARTICLE scitation.org/journal/rsi

Spatial and temporal pre-alignment of an X-ray split-and-delay unit by laser light interferometry

Cite as: Rev. Sci. Instrum. 90, 045106 (2019); doi: 10.1063/1.5089496
Submitted: 19 January 2019 • Accepted: 15 March 2019 •
Published Online: 4 April 2019

W. Roseker,[1,a)] S. Lee,[2,3,b)] M. Walther,[1] R. Rysov,[1] M. Sprung,[1] and G. Grübel[1,4]

AFFILIATIONS

[1]Deutsches-Elektronen Synchrotron DESY, Notkestr. 85, 22607 Hamburg, Germany
[2]Frontier in Extreme Physics, Korea Research Institute of Standards and Science (KRISS), Daejeon 34113, South Korea
[3]Department of Nanoscience, University of Science and Technology (UST), Daejeon 34113, South Korea
[4]The Hamburg Centre for Ultrafast Imaging, Luruper Chaussee 149, 22761 Hamburg, Germany

[a)]Electronic mail: wojciech.roseker@desy.de
[b)]Electronic mail: soobydoo@kriss.re.kr

ABSTRACT

We present a novel experimental setup for performing a precise pre-alignment of a hard X-ray split-and-delay unit based on low coherence light interferometry and high-precision penta-prisms. A split-and-delay unit is a sophisticated perfect crystal-optics device that splits an incoming X-ray pulse into two sub-pulses and generates a controlled time-delay between them. While the availability of a split-and-delay system will make ultrafast time-correlation and X-ray pump-probe experiments possible at free-electron lasers, its alignment process can be very tedious and time-consuming due to its complex construction. By implementing our experimental setup at beamline P10 of PETRA III, we were able to reduce the time of alignment to less than 3 h. We also propose an alternate method for finding the zero-time delay crossing without the use of X-rays or pulsed laser sources. The successful demonstration of this method brings prospect for operating the split-and-delay systems under alignment-time-critical environments such as X-ray free electron laser facilities.

I. INTRODUCTION

Ultrashort, extremely bright, and spatially coherent pulses from hard X-ray free-electron laser (XFEL) sources such as LCLS (USA),[1] SACLA (Japan),[2] PAL-XFEL (South Korea),[3] and European XFEL (Germany)[4] allow probing dynamics at atomic length and time scales.[5–9] For techniques such as X-ray photon correlation spectroscopy (XPCS),[10] the intrinsic time-resolution available at synchrotrons is limited by the bunch separation between successive X-ray pulses. However, since typical pulse delivery rates at FEL sources range between tens of hertz to megahertz,[11] dynamics occurring at nanosecond to femtosecond time scales cannot be accessed by using conventional methods.[12–15,34,35] This limitation can be overcome by using the double-pulse speckle contrast correlation approach,[16–20] in which a characteristic time scale of the sample dynamics is measured as a function of time delays between two probing pulses. In order to implement this approach at FEL facilities, one needs either an accelerator based double-pulse technology[21] or optical split-and-delay systems at the experimental stations. In particular, the latter one can provide continuous time-delays from femtoseconds to nanoseconds allowing us to probe ultrafast dynamics in various condensed matter systems.[22] The first optical split-and-delay systems have been operated at visible to soft X-ray wavelengths.[23–26] Equivalent devices for hard X-rays have been discussed over many years. The first hard X-ray split-and-delay system, based on the perfect crystal optics and fixed scattering geometry, has been developed at DESY.[27–29] This pioneering work paved the way to the further development and construction of split-and-delay devices at SACLA[30,31] and LCLS.[32,33] Recently, a split-and-delay system has been employed in measurements of nanosecond-equilibrium-structural dynamics of a colloidal liquid, marking the first demonstration of ultrafast XPCS.[20]

In this work, we make use of low coherence light interferometry and high-precision penta-prisms to pre-align a hard X-ray split-and-delay unit and characterize the optical path length differences between two split beams. Implementing this method allowed

us to align the split-and-delay unit in less than 3 h. We also show an alternate method for finding the zero-time delay crossing as a novel diagnostic tool for online monitoring of the time-delays between the split-pulses without the use of X-rays.

II. SPLIT-AND-DELAY LINE SETUP

The basic concept of the hard X-ray split-and-delay unit (SDU) is similar to that of a conventional optical interferometer; however, its operational principle is quite unique. Instead of using optical beam splitters (BSs) and mirrors, it utilizes combinations of single crystal Bragg reflector (BR) crystals and Bragg beam splitters (BSs) to split an incoming X-ray pulse into two parts and recombine them after introducing a controlled time-delay.[27,28] More specifically, the X-ray pulse is split by the first beam splitter crystal into two sub-pulses that propagate along two different rectangular paths, as shown in Fig. 1(a). One sub-pulse is guided via the upper optical path (referred to as upper branch), which is defined via the BR-I, BR-II, and BR-III crystals (see the inset of Fig. 1). The second sub-pulse of the beam travels through the path that is determined by the BR-IV, BR-V, and BR-VI crystals. Finally, both pulses are recombined at the beam mixer (BM) crystal and co-propagate downstream the device on the same path in the sample direction. The manipulation of the light in the hard X-ray regime is achieved by selecting appropriate crystal reflections. The pulses are reflected inside the split-and-delay unit by using perfect silicon crystal optics in a fixed 90° vertical-scattering geometry.[27,28] In order to ensure the stability of the crystal optics, a 380 kg granite support structure is constructed to hold various optical components above [see Fig. 1(a)]. An additional support structure is also built to provide a horizontal translation range of 330 mm to move the split-and-delay device in and out of the X-ray beam path.

The delay time between the two sub-pulses is given by $\Delta_t = \Delta L/c$, where ΔL is the path length difference between the upper and lower branches and c is the speed of light. It is controlled by translating a single aluminum plate, i.e., main translation unit (MTU) along the vertical plane on the axis perpendicular to the incoming beam. The MTU consists of four Bragg crystal holders mounted on the aluminum plate [see the inset of Fig. 1(a)]. The whole assembly is mounted on the translation unit, which is fixed to the granite support. For the proper operation of the split-and-delay device, X-ray beam paths inside the device need to be parallel to the plane of the MTU movement. Therefore, prior to the alignment of the crystal optics, it is necessary to adjust the entire split-and-delay granite structure with respect to the incoming beam [see Fig. 1(a)]. The use of the multiple crystal-based optical elements (6 silicon reflectors and 2 beam splitters) and relatively long path lengths inside the device require effective tools to pre-align it without X-rays and test its performance prior to the start of an actual experiment.

III. EXPERIMENTAL SETUP

The primary approach of pre-aligning split-and-delay without using X-rays is based on the idea that one can trace a virtual X-ray beam path using laser light. For this purpose, we used a HeNe laser operating at a central wavelength of 633 nm and its output is

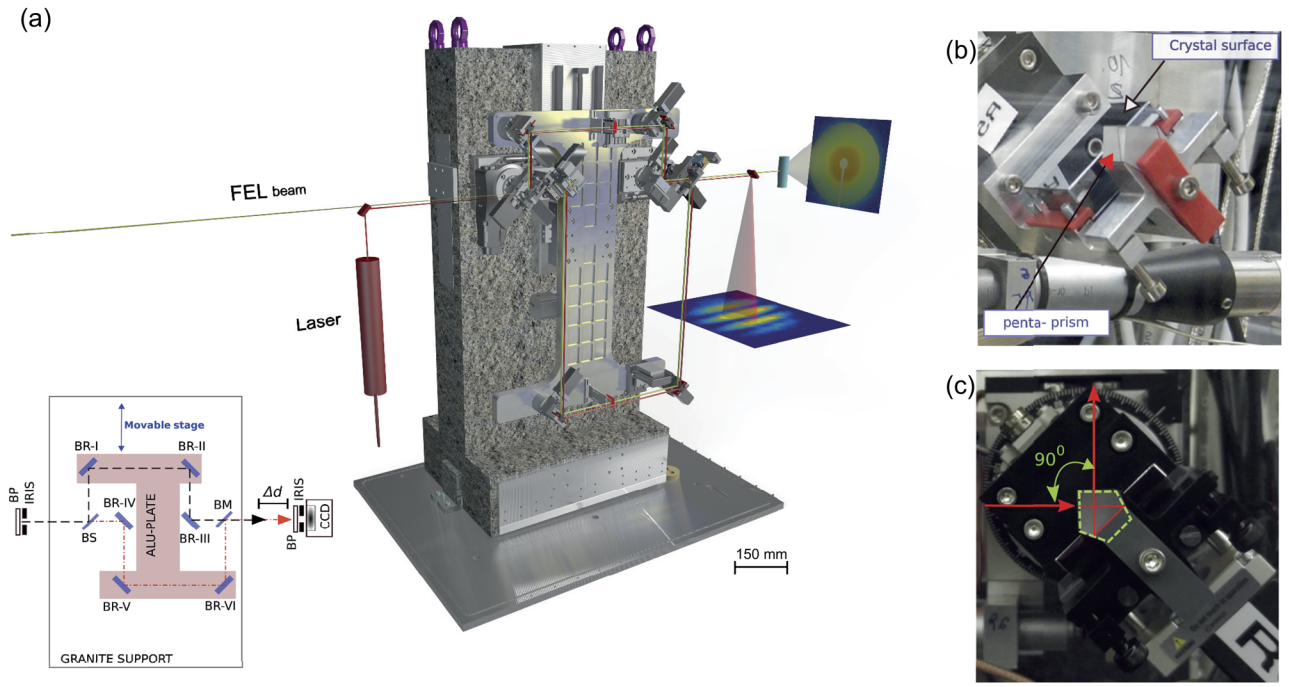

FIG. 1. (a) Illustration of the split-and-delay system in an FEL experiment together with the laser based time-delay online monitoring system. Inset: Schematic layout of the split-and-delay unit with optical components arranged in a fixed scattering geometry. (b) Custom made mount for the silicon crystal and penta-prism. (c) Optical beam propagation reflected from a penta-prism making a 90° angle between the incoming and exiting beams.

collimated via a fiber coupled optical collimator (Newport Model F-C5-F2-543) such that the precise alignment can be performed with a well defined beam size of 2 mm in diameter. Once the optical laser beam propagates co-linearly along the X-ray beam path, we adjust the split-and-delay unit such that the beam propagates on the vertical plane parallel to the surface of the granite, i.e., the distance between the beam and the granite surface at the input and output of the split-and-delay unit is kept the same. This procedure ensures that the laser beam propagates through the optics while keeping the uniform distance from the granite to the beam. As for making the 90° angles with respect to the incoming beam in the vertical plane, we use high precision optical penta-prisms (Redoptronics). The penta-prism is mostly made of glass material (fused silica/BK-7) but has a metal coating on the reflecting surfaces. It is geometrically cut such that an incoming beam always exits the crystal at 90° [see Figs. 1(b) and 1(c)]. We can emulate the X-ray beam path given that the penta-prisms are installed at appropriate crystal locations. As shown in Fig. 1(b), we built a crystal mount that holds the silicon reflector crystals and the prism at the same rotation axis but displaced apart horizontally such that we can translate the beam in and out of both the sample surface and center of the prism rotation by moving the split-and-delay unit along the horizontal axis perpendicular to the incoming beam.

IV. TEMPORAL ALIGNMENT

In order to utilize the split-and-delay unit in ultrafast time-correlation experiments, it is very crucial to find the zero-time delay (i.e., where the path length of the upper branch is equal to that of the bottom branch). In our work, we employed a low coherence interferometry technique to achieve this temporal alignment. The source in the setup is a broad bandwidth modulated red diode (Schäfter + Kirchhoff 51nanoFCM) operating at a central wavelength of 637 nm. The longitudinal coherence length of our modulated light source is about 300 μm, which corresponds to a coherence time of about 1 ps. If the path length difference ΔL is sufficiently greater than the coherence length of the source, no interference fringes will be detected. The interference pattern appears on the detection plane only when the path length difference between the two branches is within the longitudinal coherence length of the light source. In our measurement [see the inset of Fig. 1(a)], we translated the MTU stage and consequently changed the path-length differences between the two branches ΔL. Upon a change in ΔL, we observe gradual emergence and subsequent disappearance of the fringe pattern, as shown in Figs. 2(a)–2(d). To analyze the visibility of the fringes, we extracted the oscillatory component from the interference patterns by selecting 1D intensity profile I_p from the 2D fringe pattern [see Figs. 2(d) and 2(e)] and by applying a low pass filter I_f [see Fig. 2(e)] to the intensity profile I_p, according to I_p/I_f. The fringe spacing is a measure of the spatial alignment of the two beams and is described in detail in Sec. VI. The fringe visibility was calculated from the extracted fringe pattern [see Fig. 2(f)] according to

$$V = \frac{I_{max} - I_{min}}{I_{max} + I_{min}}, \tag{1}$$

where I_{max} and I_{min} denote the global maximum and minimum intensity in the entire fringe pattern, respectively. Figure 2(g) shows the visibility V as a function of the path length difference ΔL. A Gaussian curve fit to the data yields a peak visibility of 0.95 and a full-width half maximum (FWHM) of 311 ± 7 μm which is consistent with the coherence time of 1 ps. The resolution of the measurement can be improved by replacing the current laser source with a much broader band source.

V. REMOTE TIMING-CALIBRATION

While our current setup allows a viable pre-alignment of the split-and-delay unit for experiments at storage rings and FEL sources, it also offers a precise option for zero time-crossing measurements, which is highly beneficial for having a capability to monitor the time-delays between the split beams without interfering with on-going experiments. In this section, we present a novel scheme,

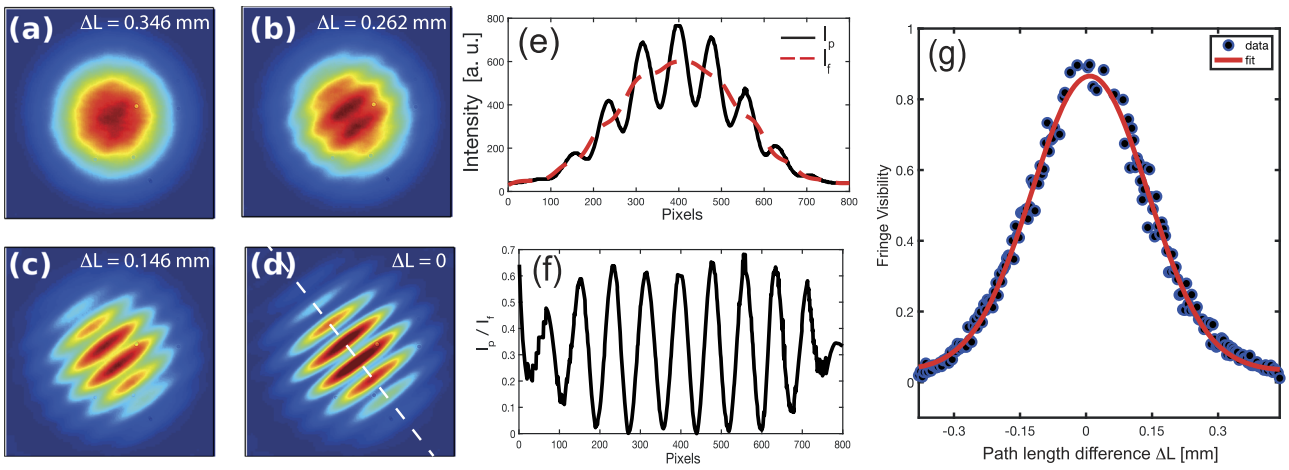

FIG. 2. [(a)–(d)] Selected interference patterns at various positions of MTU and corresponding path length differences ΔL. (e) The intensity profile (solid black line) I_p is extracted from the 2D interference pattern according to the line profile [dashed white line in (d)]. The low pass filter profile I_f is denoted by a dashed red line. (f) Extracted oscillatory component (I_p/I_f) of the recorded fringe pattern. (g) Fringe visibility as a function of the path length difference ΔL between the upper and lower branches.

which allows the measurement of the imparted time-delays without moving the main delay stage of split-and-delay. This implementation requires splitting the output from the light source and constructing an independent interferometry setup [see Fig. 3(a)]. A fraction of the modulated laser beam (hereafter referred to as a reference beam) is fed into a fiber optics and transported to the interferometry setup that is installed on a remote optical table. The rest of the beam is delivered to the split-and-delay as described in Sec. IV. However, instead of making the fringe measurement directly at the output of split-and-delay system, the exiting beams are fed into fiber optics. Typically, the most difficult part of this temporal calibration procedure is the efficient fiber coupling, which can be extremely challenging due to a small core diameter of the single mode fiber. Thus, we employ a multi-mode optical fiber which carries a relatively large core diameter of 400 μm to facilitate the light-coupling process. Here, it is important to adjust the length of the optical fiber for the reference beam such that the length of path 1 matches the length of path 2 in Fig. 3(a). Ultimately, by scanning the translation stage on the new interferometry setup, we characterize the found path-length differences between the reference beam and the two beams from the SDU. The difference between these path length differences (Δt) is equivalent to the path-length difference between the upper and lower branches. We note that the spatial beam profile after the multimode fiber will have extra interference patterns "speckle" due to propagation of multiple spatial modes. Nevertheless, we confirm that this effect is marginal as we can still obtain a clear interference pattern on CCD after the multimode fiber [see Fig. 3(b)].

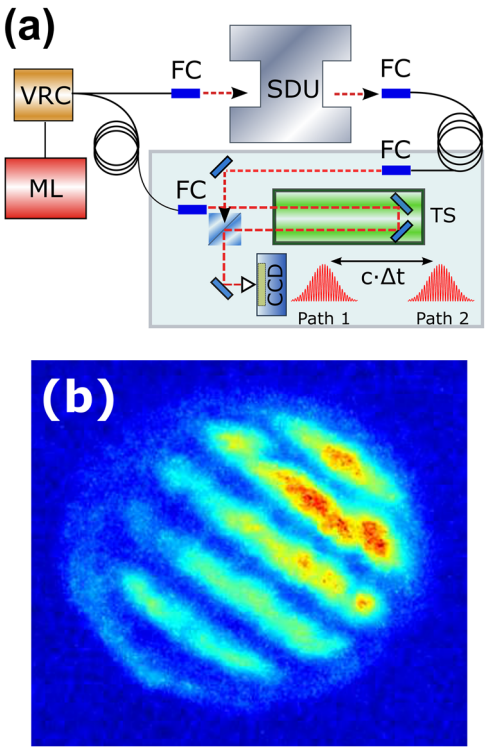

FIG. 3. (a) Schematics for the remote path-length difference calibration. ML: RF-modulated laser, VRC: variable ratio coupler, FC: fiber coupler, and TS: translation stage. (b) Interference pattern image on CCD after propagating through multimode fiber.

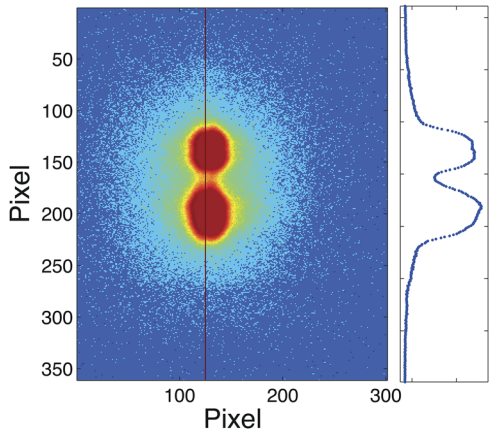

FIG. 4. An image of the throughput X-ray beams from both branches on an X-ray CCD, which was installed 17 m downstream of the split-and-delay unit at P10 beamline at PETRA III.

VI. SPATIAL ALIGNMENT

Following the preliminary alignment procedure described in Sec. III, we were able to generate Michelson fringes on an optical CCD camera with a pixel size of 5.2 μm^2 (Thorlabs CMOS camera) that is positioned after the split-and-delay-unit. By measuring the fringe spacing of the interference pattern, we were able to determine the degree of the spatial overlap between the beams exiting from both branches. More specifically, the separation between the fringe peaks corresponds to 0.4 mm in real space. In a collinear geometry, the angular misalignment between the two beams can be calculated from the fringe spacing as follows:[23,31]

$$\alpha = \sin^{-1}\left(\frac{\lambda}{\Delta D}\right), \tag{2}$$

where λ and ΔD are the laser wavelength and the fringe spacing, respectively. We measure α = 1.6 mrad, which provides a very good starting point before making the final adjustment with X-rays.

Once the optical pre-alignment procedure is completed, the split-and-delay unit is aligned to the X-ray beam. We note that it only takes minor optimization of the Bragg crystals to fine-tune X-ray diffraction intensity to finalize the alignment process. Figure 4 shows an image of two X-ray beam spots on the X-ray eye detector that is installed 17 m downstream of the split-and-delay. Centroids of the beam spots are separated by 600 μm along the y-axis, which corresponds to an angular misalignment of $\Delta\theta$ = 35 μrad. We were able to achieve the required precision typically within 3 h.

VII. CONCLUSION

We report the development of an effective procedure for pre-aligning the split-and-delay unit without using X-rays. We find that, after the alignment procedure, two-exiting beams from the upper and lower branches of the split-and-delay unit are spatially overlapped at the output and co-propagating with a marginal angular

deviation of 35 μrad. We also demonstrate the full characteristics of the path-length difference between the two branches as well as a way to find a zero time-crossing within a temporal resolution of 1 ps. The performance of the apparatus has been successfully confirmed at PETRA III with X-rays. The capability to tune the device prior to taking X-rays greatly enhances the efficient use of expensive beam times at synchrotron facilities and more importantly at X-ray FELs such as LCLS, SACLA, or European XFEL. To improve the performance of the device for an actual experiment, it will be highly beneficial to implement the remote-timing calibration scheme that was described in Sec. V of this work.

ACKNOWLEDGMENTS

Financial support by DFG within SFB 925 is gratefully acknowledged. We thank the Hamburg Centre for Ultrafast Imagining (CUI) for financial support. S.L. was supported by the National Research Foundation of Korea (No. NRF-2016K1A3A7A09005386).

REFERENCES

[1]P. Emma, R. Akre, J. Arthur, R. Bionta, C. Bostedt, J. Bozek, A. Brachmann, P. Bucksbaum, R. Coffee, F. J. Decker, Y. Ding, D. Dowell, S. Edstrom, A. Fisher, J. Frisch, S. Gilevich, J. Hastings, G. Hays, P. Hering, Z. Huang, R. Iverson, H. Loos, M. Messerschmidt, A. Miahnahri, S. Moeller, H. D. Nuhn, G. Pile, D. Ratner, J. Rzepiela, D. Schultz, T. Smith, P. Stefan, H. Tompkins, J. Turner, J. Welch, W. White, J. Wu, G. Yocky, and J. Galayda, "First lasing and operation of an angstrom-wavelength free-electron laser," Nat. Photonics **4**, 641–647 (2010).

[2]T. Ishikawa, H. Aoyagi, T. Asaka, Y. Asano, N. Azumi, T. Bizen, H. Ego, K. Fukami, T. Fukui, Y. Furukawa, S. Goto, H. Hanaki, T. Hara, T. Hasegawa, T. Hatsui, A. Higashiya, T. Hirono, N. Hosoda, M. Ishii, T. Inagaki, Y. Inubushi, T. Itoga, Y. Joti, M. Kago, T. Kameshima, H. Kimura, Y. Kirihara, A. Kiyomichi, T. Kobayashi, C. Kondo, T. Kudo, H. Maesaka, X. M. Maréchal, T. Masuda, S. Matsubara, T. Matsumoto, T. Matsushita, S. Matsui, M. Nagasono, N. Nariyama, H. Ohashi, T. Ohata, T. Ohshima, S. Ono, Y. Otake, C. Saji, T. Sakurai, T. Sato, K. Sawada, T. Seike, K. Shirasawa, T. Sugimoto, S. Suzuki, S. Takahashi, H. Takebe, K. Takeshita, K. Tamasaku, H. Tanaka, R. Tanaka, T. Tanaka, T. Togashi, K. Togawa, A. Tokuhisa, H. Tomizawa, K. Tono, S. Wu, M. Yabashi, M. Yamaga, A. Yamashita, K. Yanagida, C. Zhang, T. Shintake, H. Kitamura, and N. Kumagai, "A compact x-ray free-electron laser emitting in the sub-ångström region," Nat. Photonics **6**, 540 (2012).

[3]H.-S. Kang, C.-K. Min, H. Heo, C. Kim, H. Yang, G. Kim, I. Nam, S. Y. Baek, H.-J. Choi, G. Mun, B. R. Park, Y. J. Suh, D. C. Shin, J. Hu, J. Hong, S. Jung, S.-H. Kim, K. Kim, D. Na, S. S. Park, Y. J. Park, J.-H. Han, Y. G. Jung, S. H. Jeong, H. G. Lee, S. Lee, S. Lee, W.-W. Lee, B. Oh, H. S. Suh, Y. W. Parc, S.-J. Park, M. H. Kim, N.-S. Jung, Y.-C. Kim, M.-S. Lee, B.-H. Lee, C.-W. Sung, I.-S. Mok, J.-M. Yang, C.-S. Lee, H. Shin, J. H. Kim, Y. Kim, J. H. Lee, S.-Y. Park, J. Kim, J. Park, I. Eom, S. Rah, S. Kim, K. H. Nam, J. Park, J. Park, S. Kim, S. Kwon, S. H. Park, K. S. Kim, H. Hyun, S. N. Kim, S. Kim, S.-m. Hwang, M. J. Kim, C.-y. Lim, C.-J. Yu, B.-S. Kim, T.-H. Kang, K.-W. Kim, S.-H. Kim, H.-S. Lee, H.-S. Lee, K.-H. Park, T.-Y. Koo, D.-E. Kim, and I. S. Ko, "Hard x-ray free-electron laser with femtosecond-scale timing jitter," Nat. Photonics **11**, 708–713 (2017).

[4]T. Tschentscher, C. Bressler, J. Grünert, A. Madsen, A. Mancuso, M. Meyer, A. Scherz, H. Sinn, and U. Zastrau, "Photon beam transport and scientific instruments at the European XFEL," Appl. Sci. **7**, 592–635 (2017).

[5]B. G. Stephenson, A. Robert, and G. Grübel, "X-ray spectroscopy: Revealing the atomic dance," Nat. Mater. **8**, 702–703 (2009).

[6]S. O. Hruszkewycz, M. Sutton, P. H. Fuoss, B. Adams, S. Rosenkranz, K. F. Ludwig, W. Roseker, D. Fritz, M. Cammarata, D. Zhu, S. Lee, H. Lemke, C. Gutt, A. Robert, G. Grübel, and G. B. Stephenson, "High contrast x-ray speckle from atomic-scale order in liquids and glasses," Phys. Rev. Lett. **109**, 185502 (2012).

[7]M. Leitner, B. Sepiol, L.-M. Stadler, B. Pfau, and G. Vogl, "Atomic diffusion studied with coherent x-rays," Nat. Mater. **8**, 717–720 (2009).

[8]B. Ruta, G. Baldi, Y. Chushkin, B. Rufflé, L. Cristofolini, A. Fontana, M. Zanatta, and F. Nazzani, "Revealing the fast atomic motion of network glasses," Nat. Commun. **5**, 3939 (2014).

[9]M. Trigo, M. Fuchs, J. Chen, M. P. Jiang, M. Cammarata, S. Fahy, D. M. Fritz, K. Gaffney, S. Ghimire, A. Higginbotham, S. L. Johnson, M. E. Kozina, J. Larsson, H. Lemke, A. M. Lindenberg, G. Ndabashimiye, F. Quirin, K. Sokolowski-Tinten, C. Uher, G. Wang, J. S. Wark, D. Zhu, and D. A. Reis, "Fourier-transform inelastic x-ray scattering from time- and momentum-dependent phonon-phonon correlations," Nat. Phys. **9**, 790–794 (2013).

[10]G. Grübel and F. Zontone, "Correlation spectroscopy with coherent x-rays," J. Alloys Compd. **362**, 3–11 (2004).

[11]M. O. Wiedorn, D. Oberthür, R. Bean, R. Schubert, N. Werner, B. Abbey, M. Aepfelbacher, L. Adriano, A. Allahgholi, N. Al-Qudami, J. Andreasson, S. Aplin, S. Awel, K. Ayyer, S. Bajt, I. Barák, S. Bari, J. Bielecki, S. Botha, D. Boukhelef, W. Brehm, S. Brockhauser, I. Cheviakov, M. A. Coleman, F. Cruz-Mazo, C. Danilevski, C. Darmanin, R. B. Doak, M. Domaracky, K. Dörner, Y. Du, H. Fangohr, H. Fleckenstein, M. Frank, P. Fromme, A. M. Gañán-Calvo, Y. Gevorkov, K. Giewekemeyer, H. M. Ginn, H. Graafsma, R. Graceffa, D. Greiffenberg, L. Gumprecht, P. Göttlicher, J. Hajdu, S. Hauf, M. Heymann, S. Holmes, D. A. Horke, M. S. Hunter, S. Imlau, A. Kaukher, Y. Kim, A. Klyuev, J. Knoška, B. Kobe, M. Kuhn, C. Kupitz, J. Küpper, J. M. Lahey-Rudolph, T. Laurus, K. Le Cong, R. Letrun, P. L. Xavier, L. Maia, F. R. N. C. Maia, V. Mariani, M. Messerschmidt, M. Metz, D. Mezza, T. Michelat, G. Mills, D. C. F. Monteiro, A. Morgan, K. Mühlig, A. Munke, A. Münnich, J. Nette, K. A. Nugent, T. Nuguid, A. M. Orville, S. Pandey, G. Pena, P. Villanueva-Perez, J. Poehlsen, G. Previtali, L. Redecke, W. M. Riekehr, H. Rohde, A. Round, T. Safenreiter, I. Sarrou, T. Sato, M. Schmidt, B. Schmitt, R. Schönherr, J. Schulz, J. A. Sellberg, M. M. Seibert, C. Seuring, M. L. Shelby, R. L. Shoeman, M. Sikorski, A. Silenzi, C. A. Stan, X. Shi, S. Stern, J. Sztuk-Dambietz, J. Szuba, A. Tolstikova, M. Trebbin, U. Trunk, P. Vagovic, T. Ve, B. Weinhausen, T. A. White, K. Wrona, C. Xu, O. Yefanov, N. Zatsepin, J. Zhang, M. Perbandt, A. P. Mancuso, C. Betzel, H. Chapman, and A. Barty, "Megahertz serial crystallography," Nat. Commun. **9**, 4025 (2018).

[12]F. Lehmkühler, C. Gutt, B. Fischer, M. A. Schroer, M. Sikorski, S. Song, W. Roseker, J. Glownia, M. Chollet, S. Nelson, K. Tono, T. Katayama, M. Yabashi, T. Ishikawa, A. Robert, and G. Grübel, "Single shot coherence properties of the free-electron laser SACLA in the hard x-ray regime," Sci. Rep. **4**, 5234 (2014).

[13]F. Lehmkühler, P. Kwaśniewski, W. Roseker, B. Fischer, M. A. Schroer, K. Tono, T. Katayama, M. Sprung, M. Sikorski, S. Song, J. Glownia, M. Chollet, S. Nelson, A. Robert, C. Gutt, M. Yabashi, T. Ishikawa, and G. Grübel, "Sequential single shot x-ray photon correlation spectroscopy at the SACLA free electron laser," Sci. Rep. **5**, 17193 (2015).

[14]J. Carnis, W. Cha, J. Wingert, J. Kang, Z. Jiang, and S. Song, "Demonstration of feasibility of x-ray free electron laser studies of dynamics of nanoparticles in entangled polymer melts," Sci. Rep. **4**, 6017 (2014).

[15]F. Lehmkühler, J. Valerio, D. Sheyfer, W. Roseker, M. A. Schroer, B. Fischer, K. Tono, M. Yabashi, T. Ishikawa, and G. Grübel, "Dynamics of soft nanoparticle suspensions at hard x-ray FEL sources below the radiation-damage threshold," IUCrJ **5**, 801–807 (2018).

[16]G. Grübel, B. G. Stephenson, C. Gutt, H. Sinn, and T. Tschentscher, "XPCS at the European x-ray free electron laser facility," Nucl. Instrum. Methods Phys. Res., Sect. B **262**, 357–367 (2007).

[17]C. Gutt, L.-M. Stadler, A. Duri, T. Autenrieth, O. Leupold, Y. Chushkin, and G. Grübel, "Measuring temporal speckle correlations at ultrafast x-ray sources," Opt. Express **17**, 55–61 (2009).

[18]S. Lee, W. Jo, H. S. Wi, C. Gutt, and G. W. Lee, "Resolving high-speed colloidal dynamics beyond detector response time via two pulse speckle contrast correlation," Opt. Express **22**, 21567–21576 (2014).

[19]E. M. Dufresne, S. Narayanan, A. R. Sandy, D. M. Kline, Q. Zhang, E. C. Landahl, and S. Ross, "Pushing x-ray photon correlation spectroscopy beyond the continuous frame rate limit," Opt. Express **24**, 355–364 (2016).

[20]W. Roseker, S. O. Hruszkewycz, F. Lehmkühler, M. Walther, H. Schulte-Schrepping, S. Lee, T. Osaka, L. Strader, R. Hartmann, M. Sikorski, S. Song, A. Robert, P. H. Fuoss, M. Sutton, G. B. Stephenson, and G. Grubel, "Towards ultrafast dynamics with split-pulse x-ray photon correlation spectroscopy at free electron laser sources," Nat. Commun. **9**, 1704 (2018).

[21]T. Hara, Y. Inubushi, T. Katayama, T. Sato, H. Tanaka, T. Tanaka, T. Togashi, K. Togawa, K. Tono, M. Yabashi, and T. Ishikawa, "Two-colour hard x-ray free-electron laser with wide tunability," Nat. Commun. **4**, 2919 (2013).
[22]A. R. Sandy, Q. Zhang, and L. B. Lurio, "Hard x-ray photon correlation spectroscopy methods for materials studies," Annu. Rev. Mater. Res. **48**, 167–190 (2018).
[23]R. Mitzner, B. Siemer, M. Neeb, T. Noll, F. Siewert, S. Roling, M. Rutkowski, A. A. Sorokin, M. Richter, P. Juranic, K. Tiedtke, J. Feldhaus, W. Eberhardt, and H. Zacharias, "Spatio-temporal coherence of free electron laser pulses in the soft x-ray regime," Opt. Express **16**, 19909–19919 (2008).
[24]B. F. Murphy, J. C. Castagna, J. D. Bozek, and N. Berrah, "Mirror-based soft x-ray split-and-delay system for femtosecond pump probe experiments at LCLS," Proc. SPIE **8504**, 850409 (2012).
[25]R. Mitzner, A. A. Sorokin, B. Siemer, S. Roling, M. Rutkowski, H. Zacharias, M. Neeb, T. Noll, F. Siewert, W. Eberhardt, M. Richter, P. Juranic, K. Tiedtke, and J. Feldhaus, "Direct autocorrelation of soft-x-ray free-electron-laser pulses by time-resolved two-photon double ionization of He," Phys. Rev. A **80**, 025402 (2009).
[26]S. Roling, S. Braun, P. Gawlitza, L. Samoylova, B. Siemer, H. Sinn, F. Siewert, F. Wahlert, M. Woestmann, and H. Zacharias, "A split- and delay-unit for the European XFEL," Proc. SPIE **8778**, 87781G (2013).
[27]W. Roseker, H. Franz, H. Schulte-Schrepping, A. Ehnes, O. Leupold, F. Zontone, A. Robert, and G. Grübel, "Performance of a picosecond x-ray delay line unit at 8.39 keV," Opt. Lett. **34**, 1768–1770 (2009).
[28]W. Roseker, H. Franz, H. Schulte-Schrepping, A. Ehnes, O. Leupold, F. Zontone, S. Lee, A. Robert, and G. Grübel, "Development of a hard x-ray delay line for x-ray photon correlation spectroscopy and jitter-free pump–probe experiments at x-ray free-electron laser sources," J. Synchrotron Radiat. **18**, 481–491 (2011).
[29]W. Roseker, S. Lee, M. Walther, H. Schulte-Schrepping, H. Franz, A. Gray, M. Sikorski, P. H. Fuoss, G. B. Stephenson, A. Robert, and G. Grübel, "Hard x-ray delay line for x-ray photon correlation spectroscopy and jitter-free pump-probe experiments at LCLS," Proc. SPIE **8504**, 85040I-1–85040I-7 (2012).
[30]T. Osaka, T. Hirano, Y. Sano, Y. Inubushi, S. Matsuyama, K. Tono, T. Ishikawa, K. Yamauchi, and M. Yabashi, "Wavelength-tunable split-and-delay optical system for hard x-ray free-electron lasers," Opt. Express **24**, 9187–9201 (2016).
[31]T. Osaka, T. Hirano, Y. Morioka, Y. Sano, Y. Inubushi, T. Togashi, I. Inoue, K. Tono, A. Robert, K. Yamauchi, J. B. Hastings, and M. Yabashi, "Characterization of temporal coherence of hard x-ray free-electron laser pulses with single-shot interferograms," IUCrJ **4**, 728–733 (2017).
[32]D. Zhu, Y. Sun, D. W. Schafer, H. Shi, J. H. James, K. L. Gumerlock, T. O. Osier, R. Whitney, L. Zhang, J. Nicolas, B. Smith, A. H. Barada, and A. Robert, "Development of a hard x-ray split-delay system at the linac coherent light source," Proc. SPIE **10237**, 102370R (2017).
[33]W. Lu, T. Noll, T. Roth, I. Agapov, G. Geloni, M. Holler, J. Hallmann, G. Ansaldi, S. Eisebitt, and A. Madsen, "Design and throughput simulations of a hard x-ray split and delay line for the MID station at the European XFEL," AIP Conf. Proc. **1741**, 030010 (2016).
[34]S. Lee, W. Roseker, C. Gutt, B. Fischer, H. Conrad, F. Lehmkühler, I. Steinke, D. Zhu, H. Lemke, M. Cammarata, D. Fritz, P. Wochner, M. Castro-Colin, S. O. Hruszkewycz, P. H. Fuoss, G. B. Stephenson, G. Grübel, and A. Robert, "Single shot speckle and coherence analysis of the hard x-ray free electron laser LCLS," Opt. Express **21**, 24647–24664 (2013).
[35]S. Lee, W. Roseker, C. Gutt, Z. Huang, Y. Ding, G. Grübel, and A. Robert, "High wavevector temporal speckle correlations at the linac coherent light source," Opt. Express **20**, 9790–9800 (2012).